Experimental and Numerical Studies of a Horizontal Axis Wind Turbine Performance over a Steep 2D Hill

Ibrahim, Omar M. A. M.
Interdisciplinary Graduate School of Engineering Sciences, Kyushu University

Yoshida, Shigeo
Research Institute for Applied Mechanics, Kyushu University

https://doi.org/10.5109/1957496

出版情報：Evergreen. 5 (3), pp.12-21, 2018-09. Green Asia Education Center
バージョン：

Experimental and Numerical Studies of a Horizontal Axis Wind Turbine Performance over a Steep 2D Hill

Omar M. A. M. Ibrahim[1,*], Shigeo Yoshida[2]

[1]Interdisciplinary Graduate School of Engineering Sciences, Kyushu University, Japan

[2]Research Institute for Applied Mechanics, Kyushu University, Japan

*Author to whom correspondence should be addressed,

E-mail: omar.ibrahim@riam.kyushu-u.ac.jp

(Received January 30, 2018; accepted August 28, 2018).

Wind tunnel tests and Numerical simulations were done to study the effect of a steep two-dimensional (2D) hill on the performance of a horizontal axis wind turbine. Experiments were performed in the wind tunnel to measure the average vertical wind speed distribution over the hill and the load acted on the wind turbine at a number of locations over the hill. Flow over the 2D hill and wind turbine power coefficient were examined using Computational Fluid Dynamics (CFD) simulations where the wind turbine rotor was fully resolved. CFD simulations had a good agreement with wind tunnel test results, and current studies showed the great impact of the 2D hill on the performance of the wind turbine.

Keywords: Complex Terrains, Wind Tunnel Test, CFD, Wind Turbine Performance.

1. Introduction

Wind turbines can affect each other when they are grouped together in a wind farm. A wind turbine extracts wind kinetic energy, leading to a decrease in wind speed, therefore electricity production of the downstream wind turbine is reduced [1, 2]. Power output reduction of downstream wind turbines could be 10-40% [3-5]. Wakes of upstream wind turbines are turbulent, and can increase stresses and fatigue applied on downstream wind turbines, causing reduction of wind turbine life time [1, 2, 6].

The number of onshore wind farms has considerably increased over the last 10 years [7], and an increasing number of these farms are placed over or close to hills and mountainous terrain, because suitable flat terrain sites are already used. Complex terrains can have a negative impact on wind turbine performance and life time. Uchida et al. [8] found that “pitch control was unable to respond appropriately to the wind velocity fluctuations originated from the topography upwind of the wind farm”. Li et al. [9] reported that “the cause of the repeated failure of yaw systems for an existing operational turbine was due to highly fluctuating wind conditions caused by complex terrain”. Therefore, wind farm terrain impact must be considered along with wake effects of wind turbines during the layout optimization process.

This paper investigates the impact of a steep 2D hill on a wind turbine using wind tunnel tests and CFD. Experiments were performed in the wind tunnel of Kyushu University where the average vertical wind speed distribution was measured along the hill without a wind turbine. Then, a turbine was positioned at different locations over the 2D hill to measure the load applied to the turbine. Furthermore, CFD simulations were carried out to investigate the flow over the 2D hill and the power coefficient of a turbine placed upstream and at the top of the hill. Finally, CFD results were compared with experimental results.

2. Experimental Method

The Boundary Layer Wind Tunnel (figure 1) is a closed circuit type and can be switched to open circuit if required. The dimensions of the wind tunnel test section are 15 m long, 3.6 m wide, and 2 m high. A uniform air flow with turbulence intensity less than 0.5%, and a maximum flow speed of 30m/s can be achieved in this wind tunnel [10]. The 2D hill is represented by equation (1) and shown in Figure 2. Where Z - axis is the vertical direction, h is the 2D hill height and equals to the wind turbine rotor diameter (0.512 m), L equals to h/2S, S is the slope of the hill and equals to 0.45, and X - axis is the streamwise direction.

$$Z = h\, e^{\left[-(1/2)\left(\frac{X}{L/1.1774}\right)^2\right]} \quad (1)$$

The ceiling walls of the wind tunnel were opened at section 3, 4, and 5 (figure 1) in order to significantly reduce the blockage effects [11, 12]. Large plates were mounted on each side of the hill, as can be seen in fig.3, for modeling the two dimensional flow over the hill.

Several measurements were done at the top of the hill in order to make sure that the flow over the hill is two dimensional. The hill model was positioned at about 0.12 m from wind tunnel floor in order to impose a uniform flow condition.

There were two wind tunnel test configurations. The objective of the first configuration was to examine the flow over the 2D hill without wind turbines, as can be seen in fig.3 and 4. The inlet wind velocity was constant at 7 m/s. The average wind speed distribution was measured using a standard straight hot wire anemometer at six locations over the hill every 390 mm along the streamwise direction and vertically along the Z-axis every 20 mm. The flow velocity was measured with a sampling time of 30 seconds and a sampling frequency of 1 kHz.

The objective of the second configuration was to measure the wind turbine load, as shown in figure 5 and 6. The inlet wind velocity was the same as the first configuration. The wind turbine was placed normal to the incoming flow at six locations over the hill every 390 mm along X - axis direction. Forces acting on turbine in X, Y, and Z axes as well as moments around X, Y, and Z axes were measured using a 6-component load cell. Fig.6 shows a schematic diagram of the second configuration setup.

3. Numerical Method

3.1 Case 1: Flow over 2D hill

k–ε turbulence model was previously used for simulating flow over terrain and other applications [13-15]. However, using this method results in average turbulent kinetic energy and average wind speed [16]. Alternatively, Large Eddy Simulation (LES) model was previously used [17-19] for wind flow simulation over terrain, and was able to show flow unsteadiness. Therefore, the LES model was used in this paper for flow simulation over the steep 2D hill, and the standard Smagorinsky model [52] was used as the subgrid-scale model.

The flow over the hill was simulated using Ansys Fluent where a transient pressure-based solver was used to obtain the average vertical wind speed distribution along the hill.

Computational domain was as shown in figure 8. It had the same dimensions as the wind tunnel, and the boundary conditions were as follows: Outlet was set to pressure-outlet with an operating pressure of 101,325 Pascals and a gauge pressure equals to zero. Inlet was set to velocity-inlet type at a constant velocity of 7m/s. The hill was set to no-slip condition. The ceiling windows were set at atmospheric pressure (101,325 Pascals), and a no-slip condition was employed for side walls.

An unstructured mesh was created using Ansys Meshing. Prismatic volume cells were generated on hill surface with a growth rate of 1.2, as shown in figure 7, and the first layer thickness was specified in order for y+ to be less than 1, where y^+ is a non-dimensional distance, and can be defined by equation 2. Where y is the distance to the closest wall, u_τ is the friction velocity, and ν is the kinematic viscosity.

$$y^+ = \frac{y\, u_\tau}{\nu} \quad (2)$$

3.2 Case 2: Flow around a wind turbine

Transition Shear Stress Transport (SST) model (also called the γ - Re_θ model) was used in this paper. The transition SST model combines the transport equations of the SST k-ω and two more equations [20-24]. The Transition SST model is based on three local correlation parameters $Re_{\theta c}$, $Re_{\theta t}$, and F_{Length}. $Re_{\theta c}$ is the Critical momentum thickness Reynolds number, $Re_{\theta t}$ is the Transition onset momentum thickness Reynolds number, and F_{Length} is an empirical correlation that controls the laminar-turbulent transition region length. These three parameters were optimized as described in the work of Sørensen [24]. $Re_{\theta c}$ and F_{Length} were specified, then a number of simulation runs were done to get the optimum values for $Re_{\theta c}$ and F_{Length}. Then a second series of simulation runs were done to get the optimum value for third correlation parameter $Re_{\theta t}$.

Flow around wind turbine rotor was simulated using Ansys Fluent where a steady state solver was used for investigating wind turbine performance at different inlet wind velocity profiles.

The wind turbine rotor could be modelled as a fully resolved rotor (by building a rotor body fitted mesh) [25-33], or an actuator disk or line [34]. Modelling the fully resolved rotor is an accurate way for simulating air flow around the rotor, but, it has the highest computational cost. The actuator disk method [35-43] doesn't require the creation of the turbine rotor's body fitted mesh, however, the force applied by the actuator disk on the flow is added to the momentum equation. The actuator disk method is simpler than the fully resolved rotor method and has a lower computational cost. The actuator line method [44-51] doesn't need the creation of the body fitted mesh, but the turbine blades are replaced by forces acting on rotating lines.

In this paper, a fully resolved rotor was used in CFD simulations as shown in figure 9. An unstructured mesh that satisfies the Transition SST model limitations [20-24] was created using Ansys Meshing. Prismatic volume cells were generated on the wind turbine rotor surface with a growth rate less than 1.1, as shown in figure 10, and the first layer thickness was specified in order for y+ to be less than 1. The total number of cells was about 7.6 million cells.

The computational domain was as shown in figure 11. The hill body was not included in this case, however, the hill effect was included in the inlet boundary condition.

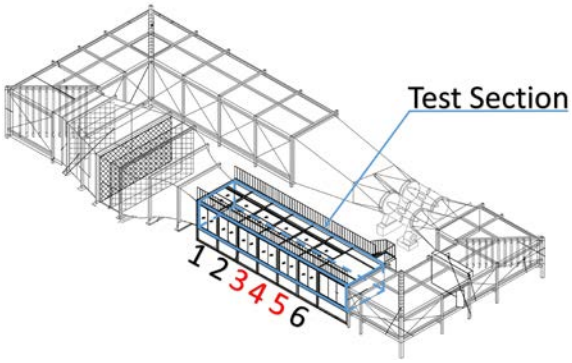

Fig. 1: Wind Tunnel of Kyushu University (Adapted from [10 and 12])

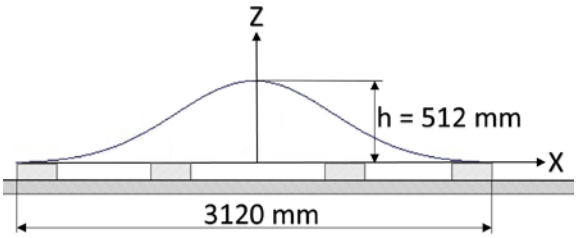

Fig. 2: Schematic diagram of the 2D hill model.

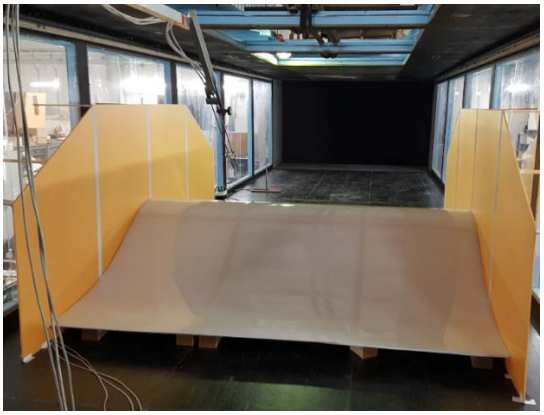

Fig. 3: Wind speed measurements over the hill.

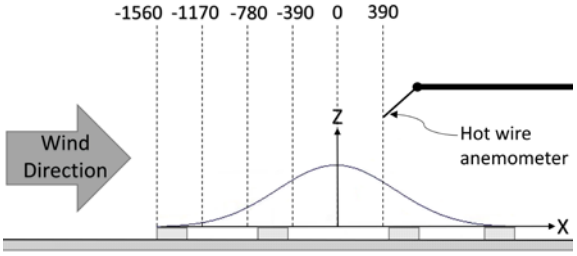

Fig. 4: Schematic diagram of the first configuration setup. Distances are in [mm].

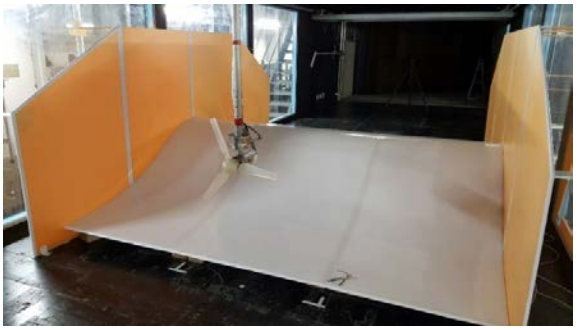

Fig. 5: Wind turbine load measurements over the hill.

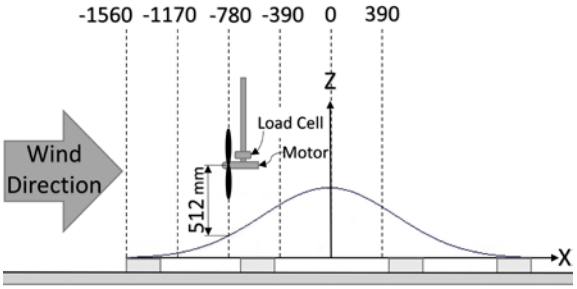

Fig.6: Second configuration setup schematic diagram.

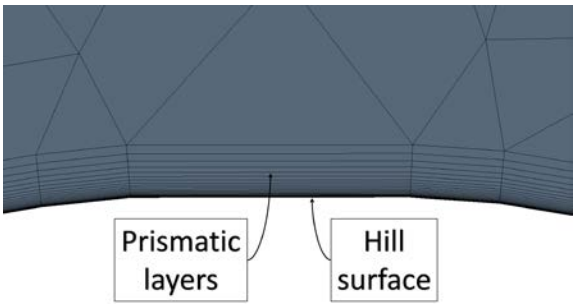

Fig.7: Prismatic layers were generated on the hill surface.

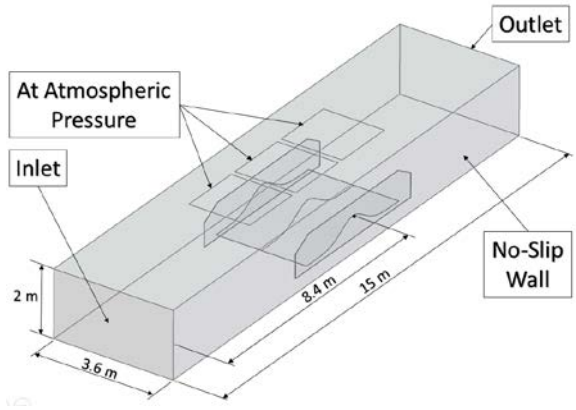

Fig. 8: Computational domain of case 1.

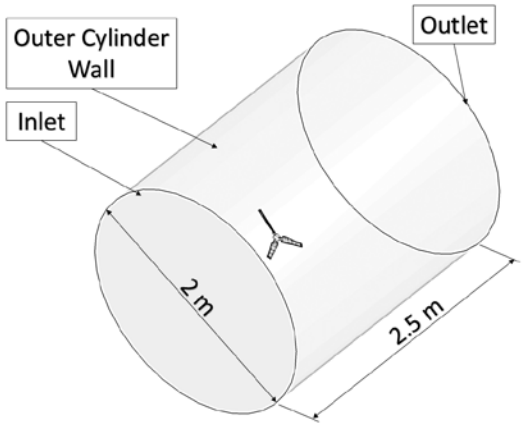

Fig. 11: Computational domain of case 2.

Fig. 9: Surface mesh of the fully resolved wind turbine rotor.

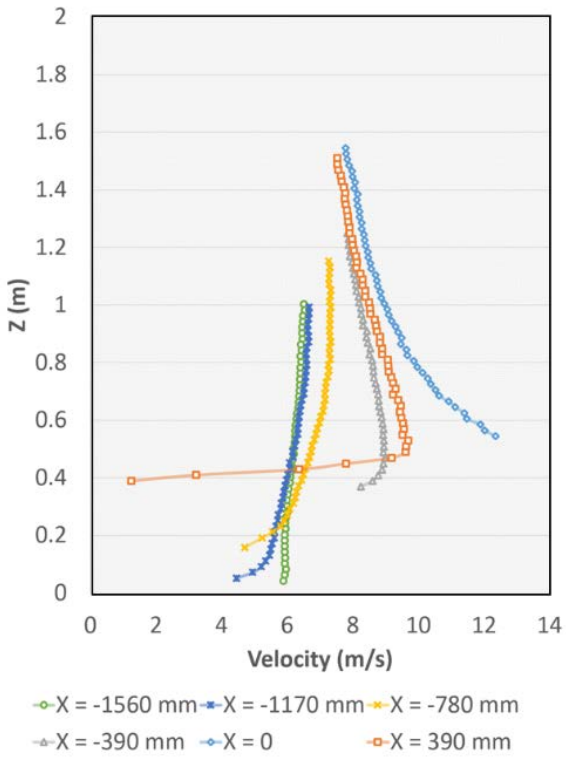

Fig. 12: Average vertical wind speed distribution over 2D hill at six locations.

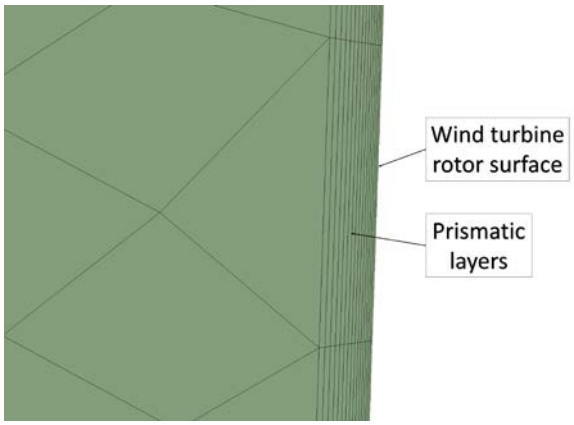

Fig. 10: Prismatic layers were generated on turbine rotor surface.

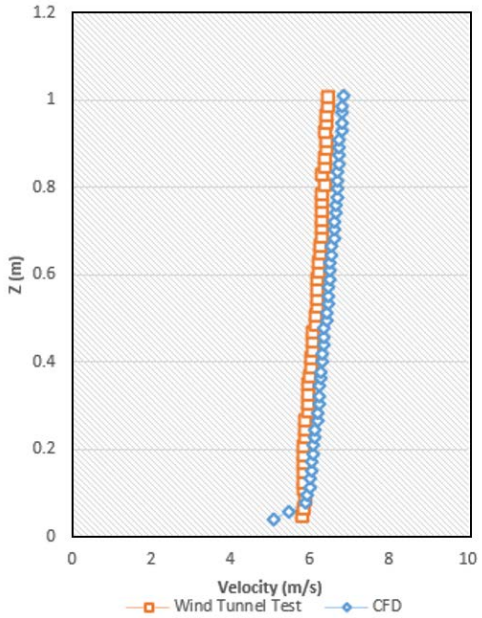

Fig. 13a: Wind speed distribution at X = -1560 mm.

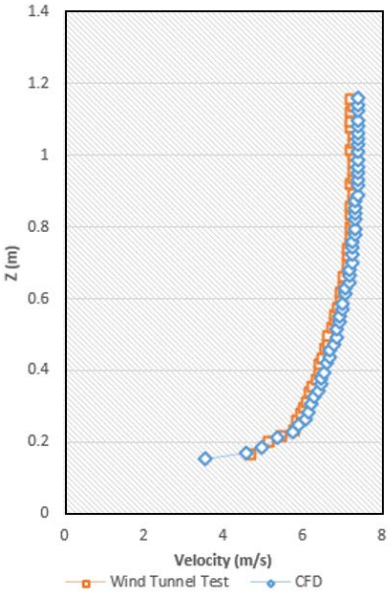

Fig. 13c: Wind speed distribution at X = -780 mm.

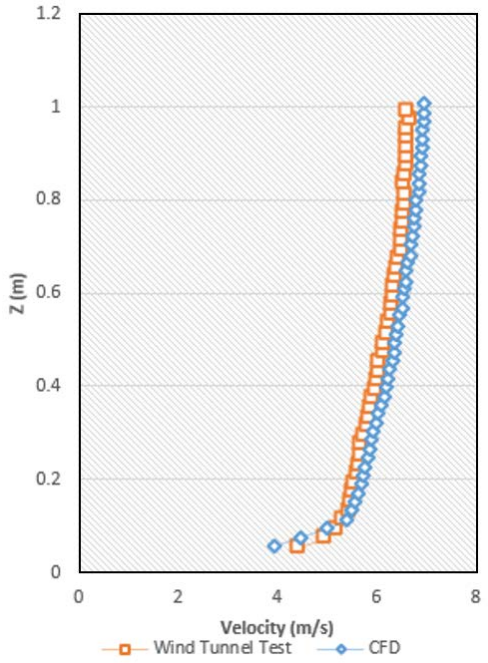

Fig. 13b: Wind speed distribution at X = -1170 mm.

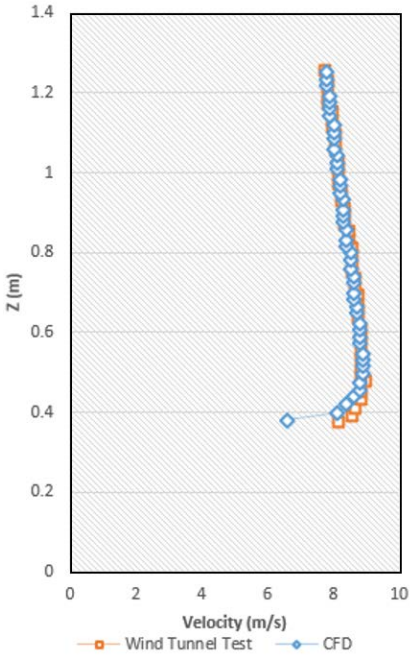

Fig. 13d: Wind speed distribution at X = -390 mm.

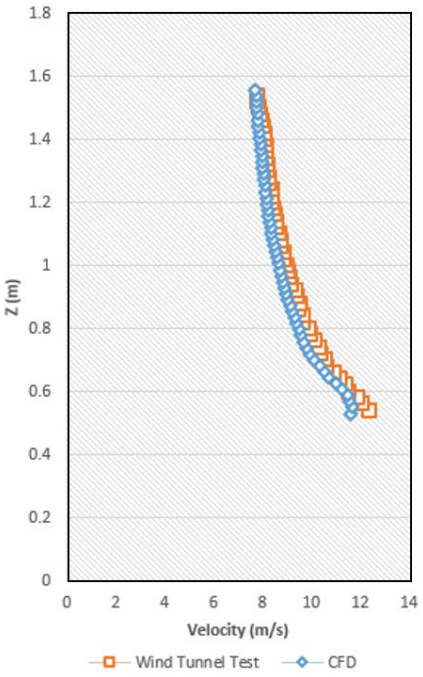

Fig. 13e: Wind speed distribution at X = 0.

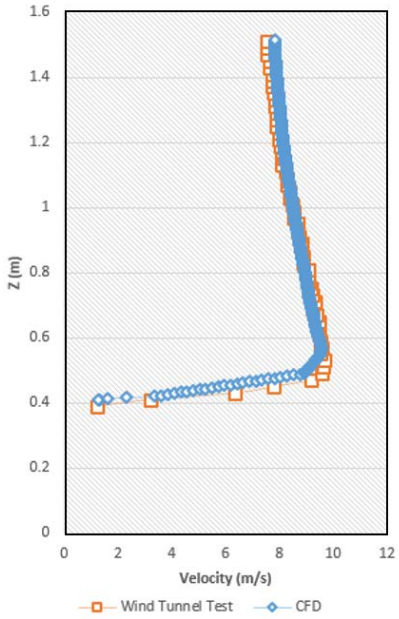

Fig. 13f: Wind speed distribution at X = 390 mm.

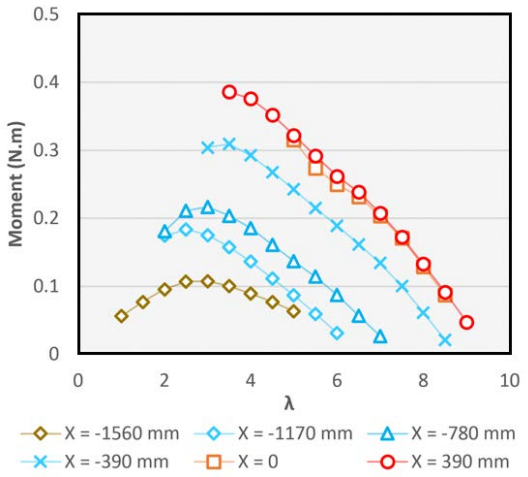

Fig. 14: Moment acting on turbine over 2D hill at six locations.

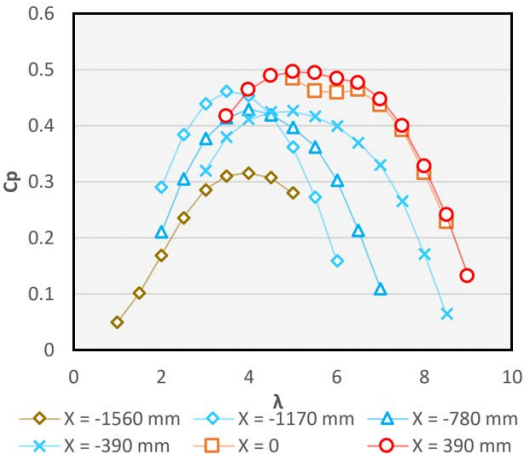

Fig. 15: Wind turbine power coefficient over 2D hill at six locations.

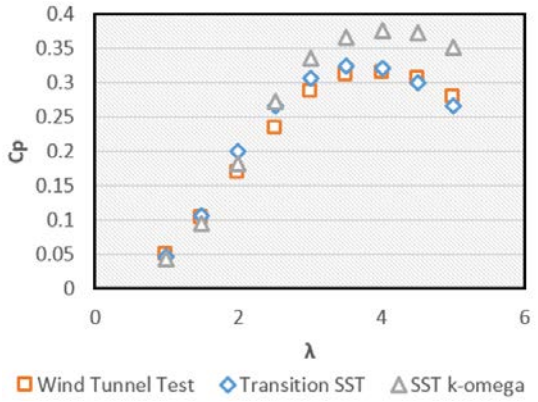

Fig. 16: Wind turbine power coefficient at X = -1560 mm.

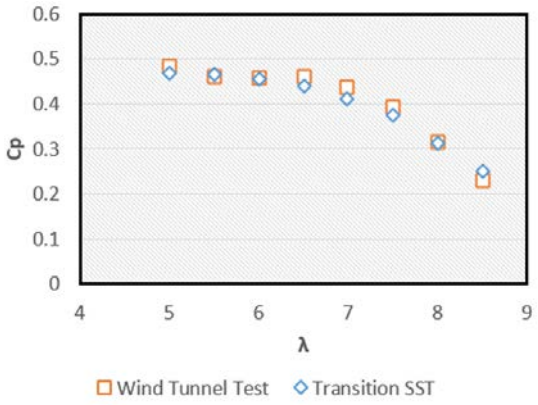

Fig. 17: Wind turbine power coefficient at X = 0.

Boundary conditions were as follows: Pressure-outlet condition was used for the outlet with an operating pressure of 101,325 Pascals and a gauge pressure equals to zero. Velocity-inlet condition was used for the inlet, and it had the same wind velocity profile as the wind tunnel test measurements. The rotor was set to no-slip condition, and the outer cylinder wall was set to symmetry type.

To simulate the rotation of the wind turbine rotor, moving reference frame was used where an axis of rotation, origin of axis of rotation, and rotational velocity were specified.

4. Results and discussion

Figure 12 shows the average vertical wind speed distribution over 2D hill at six locations starting at X = -1560 mm to X = 390 mm with an increment of 390 mm. In figure 12, the vertical axis represents the height of the wind tunnel which is equal to 2m. Wind velocity is almost constant at X = -1560 mm along the Z-direction, afterwards, wind velocity starts to increase at X = -780 mm until it reaches the maximum wind speed at X = 0, then starts to decrease at the downstream of the hill at X = 390 mm. Figure 12 shows the great effect of the steep hill on the vertical wind speed distribution. Figure 13a to 13f compare wind tunnel test results with CFD simulation. Numerical results showed a good agreement with the experimental measurements.

Figure 14 and 15 show results of the second wind tunnel test configuration. Figure 14 shows the moment acting on turbine at six locations over 2D hill versus the Tip Speed Ratio (λ). Moment acting on turbine is lowest at X = -1560 mm, and highest at X = 0 and X = 390 mm. This is due to the higher wind speed at the top of the hill compared with upstream wind speed. Power Coefficient (Cp) was calculated for the turbine at different tip speed ratios, as can be seen in figure 15. Turbine performance at the top of the hill (X = 0) and X = 390 mm was better than that at X = -1560 mm (upstream of the hill), due to the higher hub wind speed.

Figure 16 and 17 compare CFD simulations with wind tunnel test results upstream (over X = -1560 mm) and over X = 0. The Transition SST model had good agreement with experimental measurements. Predicting stall and flow separation at high tip speed ratios was possible using the Transition SST model, whereas the SST k-omega model failed to predict the stall as can be seen in Figure 16. This shows the usefulness of the Transition SST model as compared to a fully turbulent one. Therefore, the Transition SST model can be important for predicting wind turbine rotors performance.

5. Conclusions

This paper examined the flow over a steep 2D hill as well as the performance of a turbine located over the same hill. Wind velocity was almost constant at X = -1560 mm (upstream) along the Z-direction, afterwards, wind velocity started to increase at X = -780 mm until it reached the maximum wind speed at X = 0, then started to decrease at the downstream of the hill at X = 390 mm. A good agreement between Experimental and Numerical simulations was achieved for the average vertical wind speed distributions. These results displayed the impact of the steep hill on air flow.

Moment acting on turbine was lowest at X = -1560 mm (upstream), and highest at X = 0 and X = 390 mm. This is due to the higher wind speed at the top of the hill compared with upstream wind speed. A good agreement between wind tunnel test and CFD results was achieved for the wind turbine power coefficient by using the Transition SST model. The Transition SST model yielded better results than the SST k-omega turbulence model specifically at high tip speed ratios.

Abbreviations

γ	Intermittency
y	Distance to the closest wall
CFD	Computational Fluid Dynamics
SST	Shear Stress Transport
S	Slope of the hill
y^+	Non-dimensional distance
RANS	Reynolds-averaged Navier–Stokes
ν	kinematic viscosity
F_{Length}	Empirical correlation that controls the transition region length
$Re_{\theta c}$	Critical momentum thickness Reynolds number
h	Height of the hill
Cp	Power Coefficient
λ	Tip Speed Ratio
LES	Large Eddy Simulation
u_τ	Friction velocity

Acknowledgements

Green Asia program is acknowledged for the scholarship support for the first author.

References

[1] J.W. Cleijne. Results of Sexbierum Wind Farm; single wake measurements. TNO-Report 93-082, TNO Institute of Environmental and Energy Technology, (1993).

[2] P. B. S. Lissaman. Energy Effectiveness of Arbitrary Arrays of Wind Turbines, *Journal of Energy*, Vol. **3**, No. 6, pp. 323-328, (1979).

[3] H.E. Neustadter and D.A. Spera, Method for Evaluating Wind Turbine Wake Effects on Wind Farm Performance. *J. Sol. Energy Eng* 107(3), 240-243 (1985).

[4] R.J. Barthelmie, S.T. Frandsen, K. Hansen, J.G. Schepers, K. Rados,W. Schlez, A. Neubert, L.E. Jensen, and S. Neckelmann. Modelling the impact of wakes on power output at Nysted and Horns Rev. European Wind Energy Conference and Exhibition, Marseilles (2009).

[5] R. J. Barthelmie, S. T. Frandsen, O. Rathmann, E. S. Politis, J. M. Prospathopoulos, K. Rados, K. Hansen, D. Cabezon, W. Schlez, J. Phillips, A. Neubert, S. P. van der Pijl, and J. G. Schepers, Flow and wakes in large wind farms in complex terrain and offshore. American Wind Energy Association Conference, Houston, Texas (2008).

[6] Amr Mohamed Metwally Ismaiel, Sayed Mohamed Metwalli, Basman Mohamed Nabil Elhadidi, Shigeo Yoshida, Fatigue Analysis of an Optimized HAWT Composite Blade, *Evergreen*. Vol. **04**, Issue 02/03, pp. 1-6, (2017).

[7] Global Wind Energy Council (GWEC)

[8] Takanori UCHIDA, Takashi Maruyama, Hirohiko Ishikawa, Masaru Zako, and Akira Deguchi. Investigation of the Causes of Wind Turbine Blade Damage at Shiratakiyama Wind Farm in Japan — A Computer Simulation Based Approach —. *Reports of Research Institute for Applied Mechanics*, Kyushu University No.141 13 – 25, (2011).

[9] Graham Li, Susumu Takakuwa, and Takanori Uchida. Application of CFD for Turbulence Related Operational Risks Assessment of Wind Turbines in Complex Terrain. EWEA2013 Conference Proceedings. Vienna (2013).

[10] Wind Engineering Section, Research Institute for Applied Mechanics (RIAM), Kyushu University. http://www.riam.kyushu-u.ac.jp/windeng/en_index.html

[11] Yuji Ohya, Takashi Karasudani, A shrouded wind turbine generating high output power with wind-lens technology, *Energies*, 3(4), 634-649, (2010).

[12] Uli Goltenbott, Yuji Ohya, Shigeo Yoshida, Peter Jamieson. Aerodynamic interaction of diffuser augmented wind turbines in multi-rotor systems. *Renewable Energy*, 112 (2017) 25-34.

[13] G. D. Raithby, G. D. Stubley, P. A. Taylor. The Askervein Hill project: a finite control volume prediction of three-dimensional flows over the hill. *Boundary-Layer Meteorology*, 39, 247–267, (1987).

[14] Sørensen N. N. General purpose flow solver applied to flow over hills. Technical Report Risø-R-827(EN), Risø National Laboratory, (1995).

[15] B. E. Launder, D. B. Spalding. The numerical computation of turbulent flows. *Computer Methods in Applied Mechanics and Engineering*, 3 (1974) 269–289.

[16] A. Bechmann and N. N. Sørensen. Hybrid RANS/LES method for wind flow over complex terrain. *Wind Energ*. 2010; 13:36–50. (2010).

[17] Zhenqing Liu, Takeshi Ishihara, Xuhui He, Huawei Niu. LES study on the turbulent flow fields over complex terrain covered by vegetation canopy. *J. Wind Eng. Ind. Aerodyn*. 155 (2016) 60–73.

[18] J. Berg, N. Troldborg, N.N. Sørensen, E. G. Patton

and P. P. Sullivan. Large-Eddy Simulation of turbine wake in complex terrain, *J. Phys.: Conf. Ser.* 854 012003, (2017).

[19] Andreas Bechmann. Large-Eddy Simulation of Atmospheric Flow over Complex Terrain. Risø-PhD-28(EN). Risø National Laboratory. Technical University of Denmark. Roskilde, Denmark, (2006).

[20] F. R. Menter, R. B. Langtry, S. R. Likki, Y. B. Suzen, P. G. Huang, S. Völker. A correlation based transition model using local variables—part I: model formulation, *J. Turbomach* 128(3), 413-422 (2004).

[21] R. B. Langtry, F. R. Menter, S. R. Likki, Y. B. Suzen, P. G. Huang, and S. Völker. A correlation based transition model using local variables—part II: test cases and industrial applications. *J. Turbomach* 128(3), 423-434 (2004).

[22] F. R. Menter, R. Langtry, S. Völker. Transition modelling for general purpose CFD codes. *Flow Turbulence Combust* (2006) 77: 277–303.

[23] R. B. Langtry, J. Gola, F. R. Menter. Predicting 2D airfoil and 3D wind turbine rotor performance using a transition model for general CFD codes. 44th AIAA aerospace sciences meeting and exhibit, Reno, Nevada (2006).

[24] Niels N. Sørensen, CFD modelling of laminar-turbulent transition for airfoils and rotors using the γ - $\widetilde{Re}_{\theta}$ model. *Wind Energ.* 2009; 12:715–733, (2009).

[25] Frederik Zahle, Niels N. Sørensen, and Jeppe Johansen, Wind turbine rotor-tower interaction using an incompressible overset grid method. *Wind Energ.* 2009; 12:594–619, (2009).

[26] N. N. Sørensen, J. A. Michelsen, and S. Schreck. Navier–Stokes predictions of the NREL phase VI rotor in the NASA Ames 80 ft × 120 ft wind tunnel. *Wind Energ.* 2002; 5:151–169. (2002).

[27] Jang-Oh Mo, Amanullah Choudhry, Maziar Arjomandi, Young-Ho Lee. Large eddy simulation of the wind turbine wake characteristics in the numerical wind tunnel model. *J. Wind Eng. Ind. Aerodyn*. 112 (2013) 11–24.

[28] Frederik Zahle and Niels N. Sørensen. On the influence of far-wake resolution on wind turbine flow simulations. *J. Phys.: Conf. Ser.* 75 012042, (2007).

[29] E. P. N. Duque, C. P. van Dam, and S. C. Hughes. Navier-Stokes simulations of the NREL combined experiment phase II rotor. AIAA-99-0037, 37th Aerospace Sciences Meeting and Exhibit Reno, NV, U.S.A. (1999).

[30] F. Zahle and N. N. Sørensen. Overset grid flow simulation on a modern wind turbine. AIAA 2008-6727, 26th AIAA Applied Aerodynamics Conference Honolulu, Hawaii (2008).

[31] Pierre‐Elouan Réthoré, Paul van der Laan, Niels Troldborg, Frederik Zahle, Niels N. Sørensen. Verification and validation of an actuator disc model. *Wind Energ.*2014; 17:919‐937. (2014).

[32] Pierre‐Elouan Réthoré, Niels N. Sørensen, F. Zahle. Validation of an actuator disc model. EWEC 2010 Proceedings, Warsaw, Poland, (2010)

[33] J. Johansen, N. N. Sørensen, J. A. Michelsen, and S. Schreck. Detached-eddy simulation of flow around the NREL phase VI blade. *Wind Energ.* 2002; 5:185–197, (2002).

[34] B. Sanderse. Aerodynamics of wind turbine wakes. Literature review. Energy Research Centre of the Netherlands (ECN). ECN-E–09-016. (2009).

[35] E. S. Politis, J. Prospathopoulos, D. Cabezon, K. S. Hansen, P. K. Chaviaropoulos and R. J. Barthelmie, Modeling wake effects in large wind farms in complex terrain: the problem, the methods and the issues. *Wind Energ.*, 2012; 15: 161–182. doi:10.1002/we.481, (2012).

[36] J. N. Sørensen and A. Myken. Unsteady actuator disc model for horizontal axis wind turbines. *Journal of Wind Engineering and Industrial Aerodynamics*, 39:139–149, (1992).

[37] C. Masson, A. Smaïli, and C. Leclerc. Aerodynamic analysis of HAWTs operating in unsteady conditions. *Wind Energ*. 2001; 4:1–22, (2001).

[38] I. Ammara, C. Leclerc, and C. Masson. A Viscous Three-Dimensional Differential/Actuator-Disk Method for the Aerodynamic Analysis of Wind Farms. *J. Sol. Energy Eng* 124(4), 345-356, (2002).

[39] F. Castellani, A. Vignaroli, An application of the actuator disc model for wind turbine wakes calculations. *Applied Energy* 101 (2013) 432–440.

[40] J. M. Prospathopoulos, E. S. Politis, K. G. Rados, P. K. Chaviaropoulos. Evaluation of the effects of turbulence model enhancements on wind turbine wake predictions. *Wind Energ*. 2011; 14:285–300. (2011).

[41] A. Makridis, J. Chick, Validation of a cfd model of wind turbine wakes with terrain effects. *J. Wind Eng. Ind. Aerodyn*. 123 (2013) 12–29.

[42] Amina El Kasmi, Christian Masson. An extended k-ε model for turbulent flow through horizontal-axis

wind turbines. *Journal of Wind Engineering and Industrial Aerodynamics* 96 (2008) 103–122.

[43] Robert Mikkelsen. Actuator disc methods applied to wind turbines. Ph.D. thesis. Technical University of Denmark, (2003).

[44] W. Z. Shen, J. N. Sørensen, and J. Zhang. Actuator surface model for wind turbine flow computations. In Proceedings of European Wind Energy Conference 2007, Milan, (2007).

[45] I. Dobrev, F. Massouh, and M. Rapin. Actuator surface hybrid model. *J. Phys.: Conf. Ser.* 75 012019, (2007).

[46] N. Troldborg, J. N. Sørensen, and R. Mikkelsen. Actuator line simulation of wake of wind turbine operating in turbulent inflow, *J. Phys.: Conf. Ser.* 75 012063, (2007).

[47] M. Draper and G. Usera, Evaluation of the Actuator Line Model with coarse resolutions, *J. Phys.: Conf. Ser.* 625 012021, (2015).

[48] W. Z. Shen, J. H. Zhang, and J. N. Sørensen. The actuator surface model: a new Navier–Stokes based model for rotor computations, *J. Sol. Energy Eng* 131(1), 011002 (2009).

[49] Fernando Porté-Agel, Hao Lu, Yu-Ting Wu. Interaction between large wind farms and the atmospheric boundary layer. *Procedia IUTAM* 10 (2014) 307 – 318.

[50] Luis Martinez, Stefano Leonardi, Matthew Churchfield, and Patrick Moriarty. A comparison of actuator disk and actuator line wind turbine models and best practices for their use. AIAA 2012-0900, 50th AIAA Aerospace Sciences Meeting including the New Horizons Forum and Aerospace Exposition Nashville, Tennessee, (2012).

[51] N. Troldborg. Actuator line modeling of wind turbine wakes. Ph.D. thesis, Technical University of Denmark, (2008).

[52] J. Smagorinsky. General circulation experiments with the primitive equations, I. The basic experiment. *Mon. Weather Rev.* 91, 99–164, (1963).